ADVANCES IN ATOMIC, MOLECULAR AND OPTICAL PHYSICS, VOL. 53

MANIPULATING SINGLE ATOMS

DIETER MESCHEDE and ARNO RAUSCHENBEUTEL

Institut für Angewandte Physik, Universität Bonn, Wegelerstr. 8, D-53115 Bonn, Germany

Abstract

Neutral atoms are interesting candidates for experimentally investigating the transition from well-understood quantum objects to many particle and macroscopic physics. Furthermore, the ability to control neutral atoms at the single atom level opens new routes to applications such as quantum information processing and metrology. We summarize experimental methods and findings in the preparation, detection, and manipulation of trapped individual neutral atoms. The high efficiency and the observed long coherence times of the presented methods are favorable for future applications in quantum information processing.

ISSN 1049-250X
DOI 10.1016/S1049-250X(06)53003-4

1. Introduction

Neutral atoms have played an outstanding role in our understanding of the microscopic world through quantum physics. Countless details of quantum mechanics have been discovered and experimentally investigated with dilute gases of atoms. With the advent of tunable, narrowband lasers around 1970, it became possible to use laser light as an agent to control not only the internal quantum state of atoms but also the motional degrees of freedom. The first observation of individual atomic particles was successful in 1978 by P. Toschek and collaborators [1]. The experimenters realized essential premises to observe individual Barium ions: A strong electromagnetic radio frequency trap (Paul trap) to store ions in a small volume and for extended periods of time, and an efficient optical detection by resonance fluorescence from a narrowband tunable laser.

As a result of this breakthrough, trapped ions became prime objects for studying and illustrating light–matter interactions at the ultimate microscopic level, i.e., single particles interacting with well-controlled light fields. Interesting advances in the 1980s include the observation of quantum jumps [2–4], anti-bunching in resonance fluorescence [5], ion crystals [6,7], and more.

A similar degree of control was achieved for neutral atoms beginning in 1994 [8–10]. The origin for this delay with respect to ions is straightforwardly associated with the much weaker trapping forces available for a neutral atomic particle in comparison with a charged particle. Neutral atoms can be localized in space by exerting radiation pressure (magneto-optical trap, MOT), in the effective potential of an optical dipole trap (DT), or by magnetic traps (MT) if the atom carries a permanent magnetic moment. A simple calculation shows that for typical laser beam intensities trapping depths do not exceed 1 K for the MOT, 10 mK for DTs, and 1 K for typical MT designs [11].

Experimental accomplishments in handling microscopic particles since 1980 have led to the demonstration of many quantum processes at an elementary level. Perhaps even more importantly they have initiated new lines of research where the control of atomic systems—and in particular atom–atom interactions—have opened the route to study novel many particle systems. The celebrated realization of Bose–Einstein condensation with neutral atoms in 1995 [12,13] has catapulted experiments with neutral atoms into a central and unique role: they allow the study of many particle systems with tailored interactions in a highly controlled environment. It has already been shown with ultracold samples of atoms containing 10,000s of atoms, that novel quantum states, for instance, induced by quantum phase transitions, can be realized and investigated [14]. A combination of these methods with an experimental access to the atomic constituents at the single particle level promises deep insight into the physics of many particle systems and their application, e.g., in quantum simulation and quantum information processing [15].

It is the aim of this article to describe the state of art in the manipulation of single neutral atoms. It is focused on well-known optical traps for neutral atoms, usually employed for trapping much larger samples of atoms. In an alternative approach, single neutral atoms can be prepared through the interaction with a single mode of a low loss optical resonator which is of relevance for the field of cavity-QED. For more information about this field we refer to [16].

2. Single Atoms in a MOT

2.1. Magneto-Optical Trap for Single Atoms

The magneto-optical trap, proposed by J. Dalibard and realized by D. Pritchard and coworkers in 1987 [17], has revolutionized experimental work in atomic and optical physics, because it allows to directly prepare and confine cold, i.e., low velocity atoms from a background gas at room temperature. The MOT relies on spatially modulated, velocity dependent radiation pressure forces exerted by red detuned laser beams in combination with a magnetic quadrupole field. It remains to this day the work horse of physics with cold atoms and serves in nearly all experiments to initially prepare an ensemble of atoms at very low velocities.

The MOT capture rate is determined by the gradient of the magnetic quadrupole field, the diameter and the detuning of the trapping laser beams, as well as the partial pressure of the atomic species to be trapped [18]. The loss rate, on the other hand, is determined by collisions with the residual gas and exothermic intra-trap collisions. In a conventional MOT with a quadrupole field gradient of 10 G/cm, cm-wide beams, and a red detuning of the trapping laser beams of about -2γ, where γ is the natural linewidth of the atomic resonance line, typically 10^9 atoms are captured with characteristic temperatures below 1/2 the Doppler temperature. For Caesium atoms, which are used in the experiments described here, the Doppler temperature is $T_{\mathrm{Dopp}} = \hbar\gamma/2k_{\mathrm{B}} = 125\ \mu\mathrm{K}$.

Single atom preparation and observation in a MOT is achieved by taking several MOT parameters to the limits [8–10]: Since atom capture is mostly determined by the time available for radiation pressure deceleration, the trapping rate is dramatically reduced by small laser beam diameters ($\approx$1 mm) and strong field gradients (up to several 100 G/cm) [19], and of course, very low partial pressure ($<10^{-14}$ mbar) of the trapped atomic species. Very low residual gas pressure ($\approx 10^{-11}$ mbar) also makes storage times of order 1 min and more possible. In our experiment, the magnetic field gradient can be ramped up and down within typically 20–30 ms time scale which allows to actively control trap loading processes (see Section 2.3).

Resonance fluorescence is collected from a 2.1% solid angle by a self-made microscope objective with a diffraction limit below 2 μm [20], and recorded with

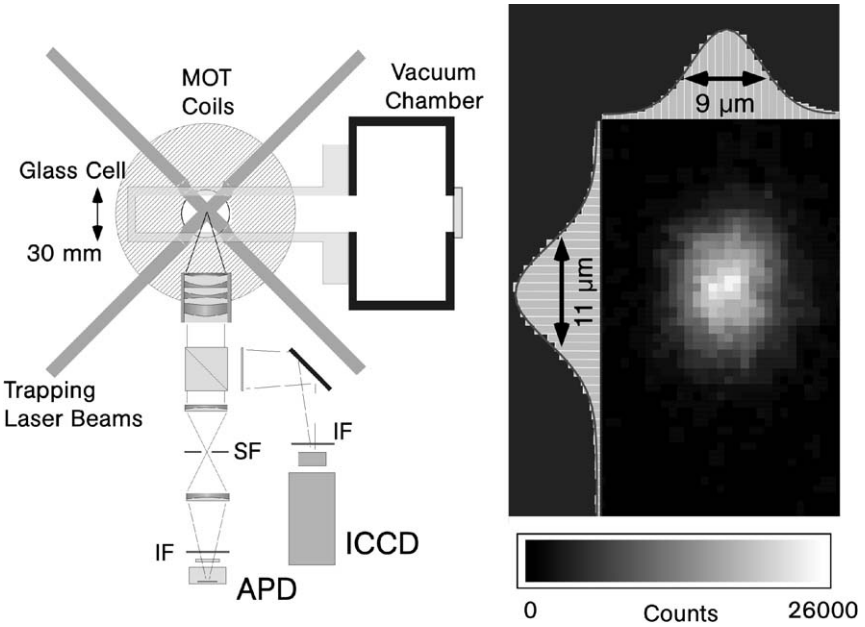

FIG. 1. Schematic of experimental setup of the magneto-optical trap. A diffraction limited microscope objective (working distance 36 mm, NA = 0.29) collects fluorescence from a 2.1% solid angle and directs half of the signal towards an intensified CCD camera (ICCD, approx. 10% quantum efficiency at 852 nm, one detected photon generates about 350 counts on the CCD chip). The other half of the fluorescence signal is transmitted by the beamsplitter and focused onto an avalanche photodiode (APD, 50% quantum efficiency). Alternatively, the ICCD can be replaced by a second APD in order to measure photon correlations (see below). The ICCD image shows the fluorescence of a single Caesium atom trapped in the MOT. One pixel corresponds to approximately 1 µm, exposure time is 1 s. Interference and spatial filters (IF, SF) are used to suppress background.

either an intensified CCD camera or with avalanche photodiodes. Spectral as well as spatial filtering helps to suppress stray light and reduces background to typically below 20,000 counts/s while the fluorescence of a single atom contributes typically $R = 60{,}000$ counts/s to the fluorescence signal. The "portrait" of a single Caesium atom illuminated with trapping laser beams at the 852 nm D2 line is shown in Fig. 1 for a 1 s exposure time.

The rate of photons recorded by the APDs reflects the time evolution of the number of trapped atoms in Fig. 2: Prominent upward steps indicate loading, downward steps disappearance of an individual atom from the trap. Neglecting background, the number of counts is proportional to the atom number N through $C_T = N \cdot f \cdot T$, where f is the fluorescence rate detected from individual atom and T is the integration time of the counter. The width ΔC_T of the individual steps in Fig. 2 is dominated, to better than 99%, by shot noise, i.e.,

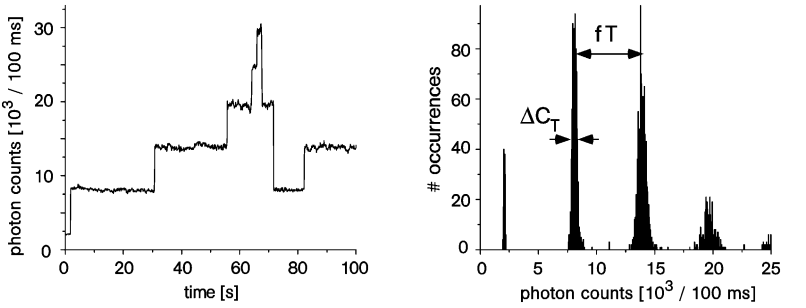

FIG. 2. Left: Time chart clip of resonance fluorescence from neutral atoms trapped in a MOT. Well-resolved equidistant fluorescence levels (step size $f \cdot T$, see text) correspond to integer numbers of atoms. Right: Distribution of count rates shows shot noise limited detection, here for an average of about 2 atoms.

$\Delta C_T \simeq \sqrt{C_T} = \sqrt{NfT}$. In order to distinguish N from $N+1$ atoms with better than 99% confidence, the step size fT must be larger than the peak widths by a factor of ≈5, i.e., $fT/5 \geqslant \sqrt{NfT}$. Thus the minimal time to detect N atoms with negligible background is $T \geqslant 25N/f$, which for $f = 6 \cdot 10^4$ results in $T \geqslant N \cdot 400$ µs, many orders of magnitude shorter than the storage and hence the processing time, see the next section.

For purely random loading and loss processes, the distribution of the occurrences for atom numbers N should exhibit a Poissonian distribution. In reality, deviations are observed as a result of atom–atom interactions as discussed below in more detail.

An interesting application of the single atom MOT has been developed by Z. Lu and coworkers [21]: The ATTA method (Atom Trap Trace Analysis) makes use of extreme selectivity of the magneto-optical trap with respect to atom species and spatial detection. The sensitivity of the method for the detection of rare species is essentially limited by the number of atoms that can be sent through the trapping volume only.

2.2. DYNAMICS OF SINGLE ATOMS IN A MOT

In the MOT, trapped atoms continuously scatter near-resonant light. During these excitation and de-excitation processes, the atoms are optically pumped from one state to another in their multilevel structure. Furthermore, due to the random transfer of momentum in each scattering event, they undergo diffusive motion in the trap volume. Finally, the interaction between atoms in the presence of near-resonant light can induce inelastic collisions causing departure from the trap.

Substantial information about all relevant dynamical processes can be retrieved from photon correlations in the resonance fluorescence which are imposed by the

atomic dynamics. We analyze photon correlations either by the classic configuration introduced by Hanbury Brown and Twiss [22], in order to overcome detector dead times at the shortest nanosecond time scale, or by directly recording photon arrival times with a computer and post-processing.

From this data, second order auto- or cross-correlation functions are derived. In the photon language, $g^{(2)}(\tau)$ describes the conditional probability to observe a second photon with a delay τ once a first photon was observed:

$$g^{(2)}_{AB}(\tau) = \frac{\langle n_A(t+\tau) n_B(t)\rangle}{\langle n_A(t)\rangle \langle n_B(t)\rangle},$$

where $\langle \ldots \rangle$ denotes time averaging, and A and B symbolize the two quantities correlated with each other.

The dynamics of a single (or a few) Caesium atoms trapped in the MOT can be derived from these measurements at all relevant time scales [23]:

(a) *Rabi-Oscillations*. Excitation and de-excitation of electronic atomic transitions occurs at the nanosecond time scale. The corresponding measurement of the auto-correlation function is shown in Fig. 3(a) and shows (after substraction of the background) the famous phenomenon of anti-bunching, i.e., the second order correlation function shows non-classical behavior at $\tau = 0$, $g^{(2)}(0) = 0$ [5,24]. Damping of the Rabi oscillations occurs at the 30 ns free space lifetime of the excited Caesium $6P$ level. The data also show that with increasing number of atoms the rate of stochastic coincidences rapidly increases: Anti-bunching can be observed at the level of a single or very few atoms only.

(b) *Optical Pumping*. It is known that optical pumping of multi-level atoms plays a central role for the realization of sub-Doppler temperatures in MOTs and optical molasses [25,26]. The single atom MOT has allowed to directly observe optical pumping by measuring, e.g., the cross-correlation $g^{(2)}_{lr}(\tau)$ for left- and right-hand circularly polarized fluorescent light, see Fig. 3(b): Observation of a lefthanded photon projects the atom into a strongly oriented quantum state from which the observation of right-handed photons is significantly reduced. Atomic motion through the spatially varying polarization of the near-resonant trapping light field induces optical pumping and causes this orientation to relax. From the data one can estimate that it takes several microseconds for an atom to travel a distance of $\lambda/2$, i.e., the length over which typical polarization variations occur.

(c) *Diffusive dynamics*. If one half of the image of the trapping volume is blocked, the intensity measured at the detector indicates the presence of the atom in the open or in the obstructed half of the trapping volume: If an atom is detected in the visible part of the MOT, it will stay there and continue to radiate into the detector until it vanishes into the oblique part by diffusion. Fig. 3(c) shows this effect in the intensity autocorrelation measurement of a single atom moving about in a MOT. A diffusion model agrees well with the observations, showing that the so-called position relaxation time is of the order of 1 ms, as directly seen from the

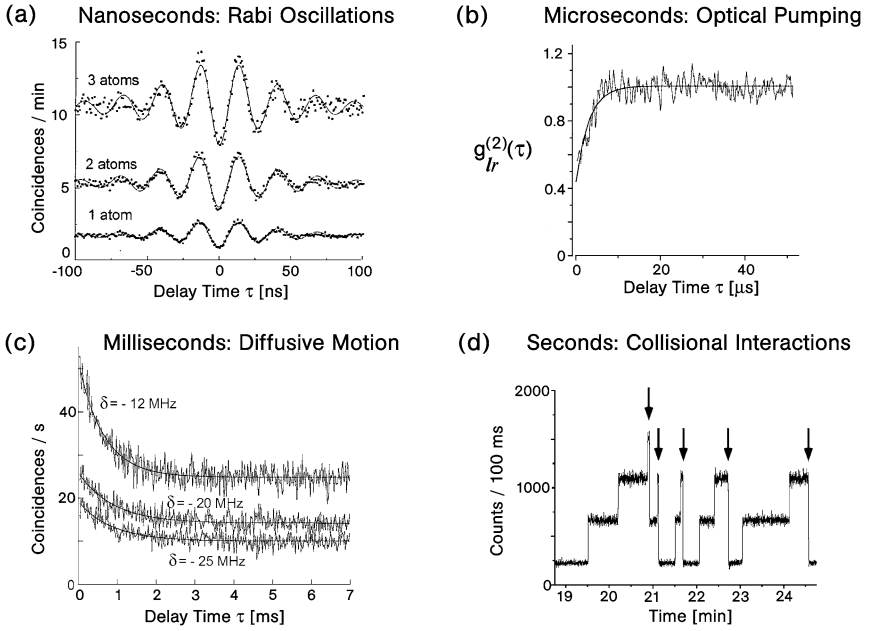

FIG. 3. Time domain measurements of atomic dynamics in a MOT by photon correlations (a)–(c) and direct observation (d). See text for details.

experimental data. The average kinetic energy and hence the diffusion constant of the atom is controlled by the detuning of the trapping laser beams.

(d) *Cold collisions*. The time chart of Fig. 3(d) shows the slow load and loss dynamics at the seconds to minutes time scale similar to the one which has already been presented in Fig. 2. One of the most interesting properties is the observation of two-atom losses (arrows), which occur much more frequently than what can be expected if one assumes Poissonian-distributed, i.e., independent, one-atom losses [27]. The analysis of the occurrence of such two-atom losses reveals that their rate is proportional to $N(N-1)$, where N is the total number of atoms trapped in the MOT. Its origin thus clearly stems from a two-body process. A detailed examination shows that inelastic collisions which are induced by the trapping laser light, so-called radiative escape processes [28], are the dominant mechanism for these two-atom losses. This experiment shows that atom–atom interactions can be observed at the level of only two atoms.

2.3. BEYOND POISSONIAN LOADING

Stochastic loading of the MOT is acceptable for applications with very small numbers of atoms. For instance, if MOT parameters are such that on average a single

atom populates the trap, Poissonian statistics predicts about 37% probability of single atom events. For many experiments, implementation of control loops does not offer a significant advantage in this case.

Some of the most interesting future routes of research with neutral atoms systems, however, will be directed towards small ("mesoscopic") systems of neutral atoms with controlled interactions. In experiments it will thus be essential to load an exactly known number of, e.g., 5–20 atoms in a much shorter time than offered by stochastic fluctuations of the atom number. In the MOT the random loading process can be manipulated by controlling the magnetic field gradient, the trapping laser beam properties, or the flux of atoms entering the trap volume. Several strategies for controlling the exact number of trapped atoms have already been investigated or are currently studied:

In the experiment by Schlosser et al. [29] an optical trap providing very strong confinement was superposed with the MOT (see also Section 3). Light assisted atom–atom interaction prevents presence of more than one atom in the trap which thus fluctuates between 0 and 1 atom occupation numbers only. Suppression of two-atom occupation of a purely magnetic trap was also observed by Willems et al. [30].

An active feedback scheme for a single Cr atom MOT has been introduced by McClelland and coworkers [31]: If the trap is empty, rapid loading ($\approx$5 ms) is achieved by directing the flux from a source of Cr atoms through light forces into the MOT volume. Using the MOT fluorescence as the indicator loading is terminated when a single atom is detected in the trap, and it is dumped if the trap contains more than one atom. An average single atom occupation probability exceeding 98% has been demonstrated in this experiment. The authors estimate that such a device may deliver individual atoms up to a rate of about 10 kHz.

In our laboratory, we have begun to explore a loading scheme, where we rapidly load a preset mean number of atoms into our MOT by temporarily lowering its magnetic field gradient. After this forced loading, the magnetic field gradient is ramped up again and the actual number of trapped atoms is determined by analyzing the level of fluorescence with a software discriminator [32]. As a result of this analysis, the atoms are either loaded into an optical dipole trap for further experiments, see Section 6, or, in case the MOT does not store the desired atom number, the atoms are discarded and the forced loading of the MOT is repeated.

3. Preparing Single Atoms in a Dipole Trap

While the MOT is an excellent device for the preparation of an exactly known number of neutral atoms, it relies on spontaneous scattering of near-resonant laser light which is highly dissipative and makes precise quantum state control of the trapped atoms impossible. We have found in our experiments that preparation of

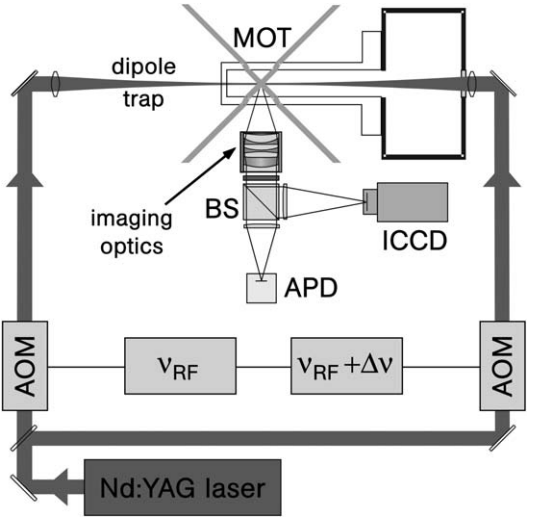

FIG. 4. Scheme of the experimental set-up. See text for details.

a sample of an exactly known number (1–30) of atoms in a MOT and subsequent transfer to an optical dipole trap (DT) makes a very efficient instrument for experiments investigating quantum control of small ensembles of neutral atoms. A very tightly confining dipole trap for similar objectives was demonstrated by Schlosser et al. [29].

In our experiment (Fig. 4), the DT is generated by a focused and far off resonant Nd:YAG or Yb:YAG laser beam at $\lambda = 1.06$ μm and 1.03 μm, respectively. The laser beam is split into two arms and can be used in a single beam configuration (traveling wave), or in a configuration of two counterpropagating beams (standing wave). We routinely reach transfer efficiencies from the MOT into the DT and vice versa in excess of 99% [33]. The dipole trap provides an approximately conservative, harmonic potential with bound oscillator quantum states for the neutral atoms. Focusing of the trapping laser beam power of several Watts to a 10–30 μm waist provides strong confinement of the atom in the transverse direction, and application of a standing wave with 0.5 μm modulation period exerts even stronger forces in the longitudinal direction. The dipole trap provides a typical potential depth of order $U_{\mathrm{Trap}}/k \approx 1$ mK. After transfer from the MOT, we measure temperatures of 50–70 μK, significantly below the 125 μK Doppler temperature for Caesium atoms [34]. Sub-Doppler cooling is enhanced during transfer from the MOT into the dipole trap since the atomic transition frequencies are light shifted towards higher frequencies and hence the cooling lasers are effectively further red detuned.

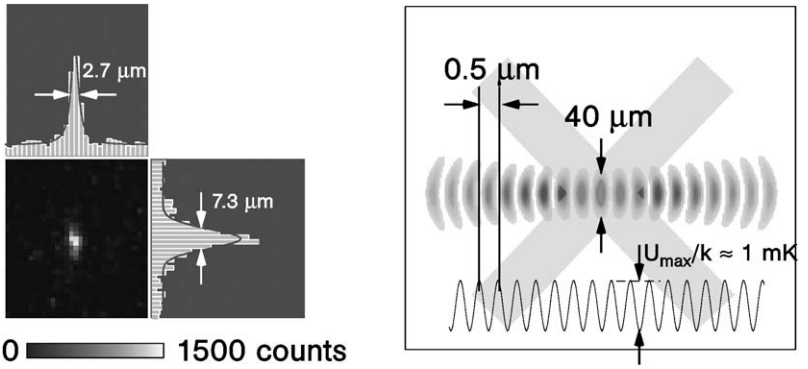

FIG. 5. Left: ICCD-image of atomic fluorescence in the optical dipole trap under continuous illumination with molasses beams, exposure time 0.5 s. In the horizontal direction, the width of the fluorescent spot is determined by the resolution of our imaging system. In the vertical direction the spot shows the extension of atomic trajectories corresponding to a temperature of about 50–70 µK in the trap of depth 1 mK. Right: Characteristic parameters of the dipole trap. Shaded areas schematically indicate MOT and molasses laser beams.

We have also realized a method to continuously illuminate an atom in the dipole trap with an optical molasses and to observe its presence through fluorescence detection. The laser cooling provided by the molasses in this case balances the heating forces. In Fig. 5 we show an ICCD image of a trapped atom as well as characteristic parameters of the dipole trap.

4. Quantum State Preparation and Detection

Neutral atoms are considered to be one of several interesting routes towards the implementation of quantum information processing. Fundamental information processing operations such as the famous quantum CNOT gate must be realized through physical interaction of the qubits [35]. For neutral atoms, several concepts, including photon exchange mediated by cavity-QED [36–38], or cold collisions [39,40] have been proposed. Each of these concepts relies on tight control of the quantum evolution of atomic qubits which already poses important experimental challenges.

In our experiments, hyperfine ground states of the Caesium atom are employed as qubits, the elementary units of quantum information storage. It is well known from the Caesium atomic clock that the microwave transition operated at $\nu_{\mathrm{hfs}} = 9.2$ GHz between the long lived $|F = 4\rangle$ and $|F = 3\rangle$ hyperfine states provides

efficient means of internal quantum state manipulation. It is thus expected that specific hyperfine states of the Caesium atom are excellent candidates to serve as qubit states with, e.g., $|0\rangle = |F = 4\rangle$ and $|1\rangle = |F = 3\rangle$. The first step in these applications is to prepare and detect ("write" and "read") arbitrary quantum state into Caesium prepared in the DT.

During the transfer from the MOT into the dipole trap, an atom is normally prepared in the $|F = 4\rangle$ state. This is achieved by switching off the MOT cooling laser, near resonant with the $|F = 4\rangle \rightarrow |F' = 5\rangle$ transition, a few milliseconds before switching off the MOT repumping laser, resonant with the $|F = 3\rangle \rightarrow |F' = 4\rangle$ transition. After this transfer, we can populate the $|F = 4, m_F = 0\rangle$ magnetic substate using resonant optical pumping on the $|F = 4\rangle \rightarrow |F' = 4\rangle$ and $|F = 3\rangle \rightarrow |F' = 4\rangle$ transition of the $\lambda = 852$ nm D2-line multiplet for about 5 ms with linear π-polarized light. In the $m_F = 0$ states, the influence of ambient magnetic field fluctuations is strongly suppressed, a favorable condition for the observation of long dephasing times described in Section 5. On the other hand, using circular σ^--polarized light, atoms can be pumped to the $|F = 4, m_F = -4\rangle$ state. This state allows fine tuning of its energy level by external magnetic fields which is essential for position selective addressing and the implementation of a neutral atom quantum register (see Section 7). Finally, an initial pure $|F = 3\rangle$ quantum state can be prepared by switching off the MOT repumping laser about 10 ms before switching off the MOT cooling laser. In this way, the $|F = 4\rangle$ state is depleted while transferring the atom from the MOT into the DT. In our trap, residual light scattering of the DT lasers causes relaxation of the hyperfine state populations of the $|F = 3\rangle$ and $|F = 4\rangle$ Caesium ground states at a time scale of several seconds or more, depending on the trapping laser intensity.

For unambiguous detection of the hyperfine state of the trapped atoms, we currently use a destructive "push-out" method [41], which discriminates the $F = 3$ and $F = 4$ levels with excellent contrast of better than 1:200 (Fig. 6). Discrimination is realized by ejecting atoms from the trap if and only if they are in the $F = 4$ state and by monitoring the presence or absence of the atom after this procedure. For this purpose, a saturating laser beam resonant with the $F = 4 \rightarrow F' = 5$ cycling transition is applied transversely to the dipole trap axis. When the trap depth is lowered to approximately 0.12 mK, atoms in $F = 4$ are pushed out in less than 1 ms by scattering on average 35 photons. Atoms in the $|F = 3\rangle$ state are not affected by the push-out laser. In the last step, the remaining atoms are either detected at a given dipole trap site by imaging with the ICCD camera, or by observing their fluorescence after recapture in the MOT. A fluorescing site indicates projection to the $F = 3$ quantum state, an empty site that was occupied before is equivalent to projection to the $F = 4$ quantum state.

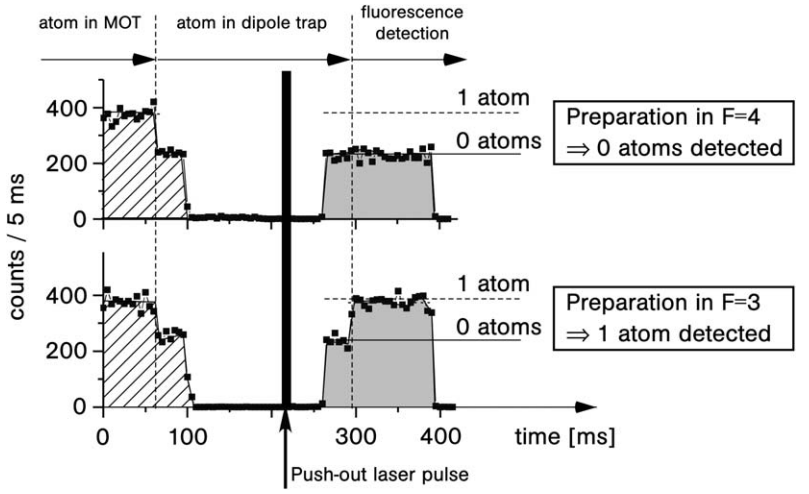

FIG. 6. Detecting the quantum state of a single neutral atom. Upper trace: An atom is prepared in the MOT and transferred to the dipole trap in state $|F = 4\rangle$. A resonant push-out laser removes the atom from the trap. When the MOT lasers are switched on again, stray light is observed only. Lower trace: In the dipole trap, the atom is transferred to the dipole trap in state $|F = 3\rangle$. The push-out laser is invisible for an atom in $|F = 3\rangle$. After switching on the MOT lasers the 1 atom fluorescence level is recovered. See text for details on atom state preparation.

5. Superposition States of Single Atoms

The two hyperfine states form a pseudo spin-1/2 system, which can be manipulated by spin rotations, induced by shining in microwave radiation resonant with the atomic clock transition. For instance, spin-flips are caused by so-called π-pulses ($|0\rangle \stackrel{\pi}{\rightarrow} |1\rangle, |1\rangle \stackrel{\pi}{\rightarrow} -|0\rangle$), where for a given magnetic field amplitude $B_\perp$ and transition moment μ the microwave pulse duration τ is defined by $\Omega\tau = (\mu B_\perp/\hbar)\tau = \pi$. We have found that in our geometrically complex apparatus, the power of our 33 dBm microwave source is most efficiently directed at the experimental region with a simple open ended waveguide. We find a minimal pulse length of 16 μs for a π-pulse. Arbitrary quantum state superpositions $\cos(\Omega\tau/2)|0\rangle + e^{i\phi}\sin(\Omega\tau/2)|1\rangle$ can be generated by varying the pulse area $\Omega\tau$ and phase ϕ, and a $\pi/2$-pulse generates superpositions with even contributions of the two quantum eigenstates.

Future applications of the trapped atom quantum states as qubits depend crucially on the question whether coupling to the environment ("decoherence") or to technical imperfections and noise ("dephasing") can be suppressed to such a degree that coherent quantum evolution is preserved at all relevant time scales.

Promisingly long coherence time in dipole traps have been first observed by Davidson et al. [42].

In the Bloch vector model, the longitudinal and transversal relaxation time constants T_1 and T_2, are introduced phenomenologically. T_1 describes the relaxation of the population difference of the two quantum states to their thermal equilibrium, T_2 the relaxation of the phase coherence between the two spin states. While spontaneous decay is completely negligible, the hyperfine state of the Caesium atom can be changed by spontaneous Raman scattering. In our current setup, we measure typically $T_1 \geqslant 3$ s [33]. With the exception of the trap life time of order 1 min this time is longer than all other relaxation times. It can be further increased by reducing the trapping laser power.

Several mechanisms contribute to transversal relaxation described by the time constant T_2. Here, we distinguish *reversible* contributions with time constant T_2^* arising from inhomogeneities of the measured ensemble, and *irreversible* contributions (T_2'), which affect the ensemble homogeneously. The total transversal relaxation time constant is thus composed of two different time constants with $T_2^{-1} = T_2^{*-1} + T_2'^{-1}$. Using Ramsey's method of separated oscillatory fields [43] we have experimentally determined the atomic coherence properties with regard to dephasing in the dipole trap [44]. A detailed analysis can be found in [41].

Figure 7 shows an example of Ramsey spectroscopy, i.e., the evolution of the $m_F = 0$ hyperfine state under the action of two $\pi/2$ microwave pulses as a function of the delay time between the pulses. If the microwave is resonant with the hyperfine transition, one expects perfect transfer from one to the other hyperfine state. The "Ramsey-fringes" observed here result from a small, intentional detun-

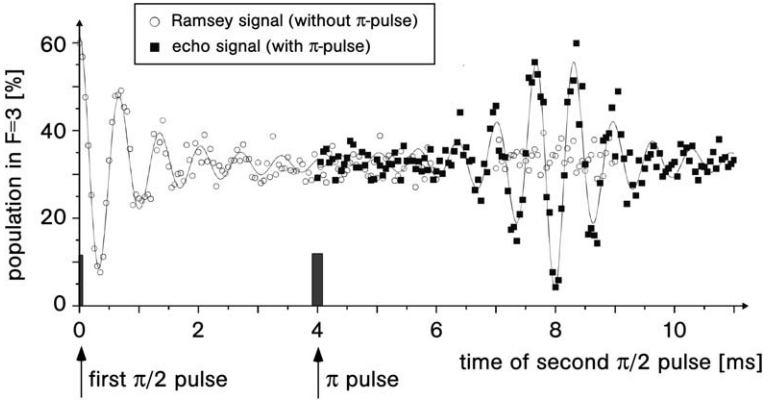

FIG. 7. Population oscillation showing hyperfine coherences of optically trapped Caesium atoms: Dephasing Ramsey fringes and spin echo signal. The $|F = 3, m_F = 0\rangle$ state is coupled to the $|F = 4, m_F = 0\rangle$ state by 9.2 GHz microwaves. The solid line corresponds to a theoretical prediction based on the thermal energy distribution of the atoms in the dipole trap only. For details see [41,44].

ing from perfect resonance. The initially observed coherent oscillation collapses after a dephasing time $T_2^* \approx T_2$, where longer dephasing times are observed for more shallow dipole potentials. This dephasing is caused by the thermal distribution of atomic motional states in the dipole trap which causes an inhomogeneous distribution of light shifts: "Cold" atoms with low kinetic energy near the potential minimum, or intensity maximum of the dipole trap experience on average stronger light shifts than "hot" atoms with larger kinetic energy.

The phase evolution of the internal atomic quantum state depends on the external, motional degrees of freedom since binding forces are caused by the light shift of the internal energy levels. Since the two hyperfine states $F = 3$ and $F = 4$ experience a small but significant relative light shift of order $\nu_{\mathrm{hfs}}/\nu_{\mathrm{D2}} = \eta \simeq 10^{-4}$, the phase evolution of any superposition state is affected by this difference and causes dephasing depending on the trajectory of the atom in the trap. In a semiclassical model, we have assumed that the free precession phase accumulated by an atomic superposition state between the two $\pi/2$-pulses depends on the average differential light shift only and calculated the thermal ensemble average yielding the solid line in Fig. 7. A quantum mechanical density matrix calculation of the same observable reproduces this result within a few percent. The deviation can be attributed to the occurrence of small oscillator quantum numbers $n_{\mathrm{osc}} \simeq 7$ in the stiff direction of the trap. We find that the envelope of the collapse of the initial oscillation corresponds to the Fourier transform of the thermal oscillator state distribution [41].

It is known that a "spin-echo" can be induced by application of a rephasing pulse [45]. Application of a π-pulse at time T_π induces an echo of the Ramsey signal with a maximum amplitude at time $2T_\pi$. The revival of the oscillation is also shown in Fig. 7. We have measured a $1/e$ decay time $T_2' \leqslant 0.15$ s for the revival amplitude. We have experimentally analyzed in detail the origin of this irreversible decay. We have found that currently the dominating sources of decoherence are the lack of beam pointing stability as well as intensity fluctuations of the trapping laser beams, while other effects such as magnetic field fluctuations and heating are negligible [41]. All relevant relaxation and dephasing times are recapitulated in Table I. Since no fundamental source of decoherence has been found which could not be reduced by technical measures, it should be possible to further increase the time span of coherent quantum evolution of the trapped atoms.

Alternatively, we have also employed resonant two-photon Raman transitions in order to introduce pseudo-spin rotations. In Fig. 8 we show a measurement of population oscillations (Rabi oscillations) between the $F = 4$ and $F = 3$ Caesium hyperfine ground states [46]. Efficient two-photon Rabi rotations are already achieved with relatively low power levels below 1 mW in each laser beam, e.g., in Fig. 8 the two-photon Rabi frequency exceeds 10 kHz. It is routine today to use focused Raman laser beams in order to address an individual particle out

Table I
Measured hyperfine relaxation times of atoms in our dipole trap

T_{relax}	$U_{\max}/k$ (mK)	m_F	Value	Limiting mechanism
T_1	1	0, −4	8.6 s	spontaneous Raman scattering
T_2^*	0.1	0	3 ms	thermal motion, scalar light shift
	0.04	0	19 ms	thermal motion, scalar light shift
	0.1	−4	270 μs	thermal motion, vector light shift
T_2'	0.1	0	34 ms	beam pointing instability
	0.04	0	150 ms	beam pointing instability
	0.1	−4	2 ms	without gradient: thermal motion, vector light shift
	0.1	−4	600 μs	with gradient: thermal motion, inhomogeneous magnetic field

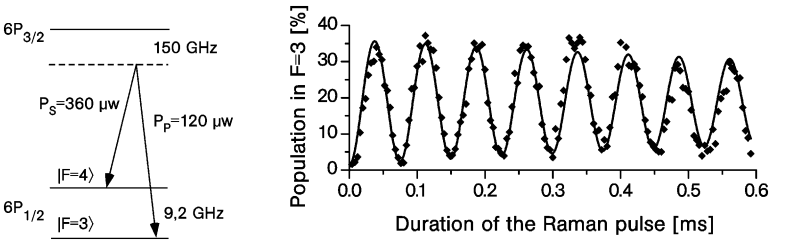

FIG. 8. Population (Rabi) oscillation showing hyperfine coherences of optically trapped Caesium atoms induced by resonant two-photon Raman transitions [46]. On the left side, details of the Caesium quantum states involved and the power levels of the Raman laser beams are given.

of a string of trapped ions [47] and to induce quantum coherences. This method, which has significantly contributed to the first successful operations of fundamental quantum gates with in these systems [48,49], is straightforwardly transferred to systems of neutral atoms. However, in Section 7 we will show that, with neutral atoms, a gradient method providing spatial resolution via spectral resolution can be applied which eliminates the need for focused laser beams.

6. Loading Multiple Atoms into the Dipole Trap

When atoms are transferred from the MOT into the dipole trap, they are distributed randomly across a 10 μm stretch of the standing wave, corresponding to

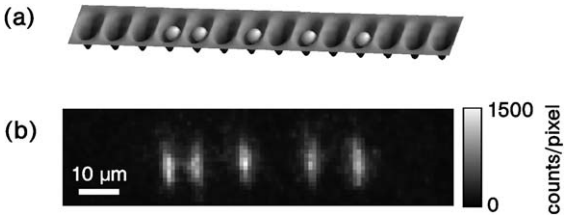

FIG. 9. (a) After the transfer from the MOT, the atoms are trapped in the potential wells of the standing wave dipole trap at random positions. The spatial period of the schematic potential wells is stretched for illustration purposes. (b) Fluorescence image of five optically resolved atoms in the standing wave dipole trap (trap axis is horizontal) after the 1D expansion detailed in the text. Integration time is 0.5 s.

about 20 antinodes or potential wells. With 5 atoms, the average separation is only 2 μm, too small to be optically resolved by our imaging system.

In order to improve the addressability, we have adopted a modified transfer procedure: After the transfer from the MOT into the standing wave dipole trap, formed by the two counterpropagating laser beams, we switch off one of the two beams within 1 ms. The potential of the resulting running wave dipole trap, created by one focussed laser beam, has Lorentzian shape with a FWHM of about 1 mm in the longitudinal direction. We let the atoms expand longitudinally for 1 ms such that they occupy a length of $\approx$100 μm. Then, we switch the second trapping laser beam on again within 1 ms, so that the atoms are "arrested" by the standing wave micropotentials at the position they have reached during the expansion. Exposure to the optical molasses warrants low temperatures of the trapped atoms. The 5 fluorescent spots in Fig. 9 correspond to a single atom each, spread out across 50 μm in this case with easily resolvable spatial separations.

As has been pointed out in Section 2.3, we have recently started to operate a feedback scheme for loading a preset number of atoms into our DT. For this, the MOT is rapidly loaded with a selectable mean number of atoms, which are only transferred into the DT if the desired number of atoms is detected in the MOT. This is particularly useful if one seeks to carry out experiments with a larger number (>3) of atoms. In this case, loading the DT with a Poissonian distributed number of atoms and postselection of the events with the desired atom number dramatically increases data acquisition time. First results obtained with this scheme are presented in Fig. 10: Part (a) shows the accumulated unconditional MOT fluorescence histogram for a large number of MOT loading cycles with a mean atom number of about 3. Part (b), on the other hand, corresponds to those events, where three atoms have been detected in the MOT, loaded into the DT, and retransferred into the MOT. The resulting conditional histogram clearly shows that we manage to controllably load three atoms into the DT with a good efficiency. In the course of these experiments, we have also found that single atom

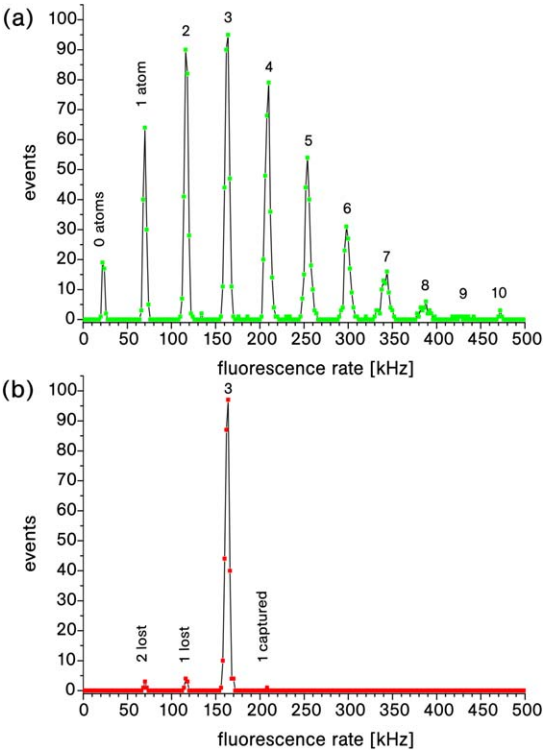

FIG. 10. Selectively loading 3 atoms. (a) Binned fluorescence signal detected by the APD after a large number of MOT loading processes. Part (b) contains all events, where three atoms were detected by the feedback loop. These atoms were then transferred into the DT and back into the MOT, see text for details.

occupation of the 1D lattice sites is generally preferred over multiple occupation favoring a regular, non-Poissonian distribution of the atoms. Details will be published in [32].

7. Realization of a Quantum Register

A quantum register consists of a well-known number of qubits that can be individually addressed and coherently manipulated. Our quantum register is composed of a string of neutral atoms, provided by the procedures described in the previous sections, which can be selectively prepared in arbitrary quantum states.

In ion traps selective addressing is achieved by means of focused Raman laser beams [47]. As discussed in Section 5, we have shown that Raman pulses can

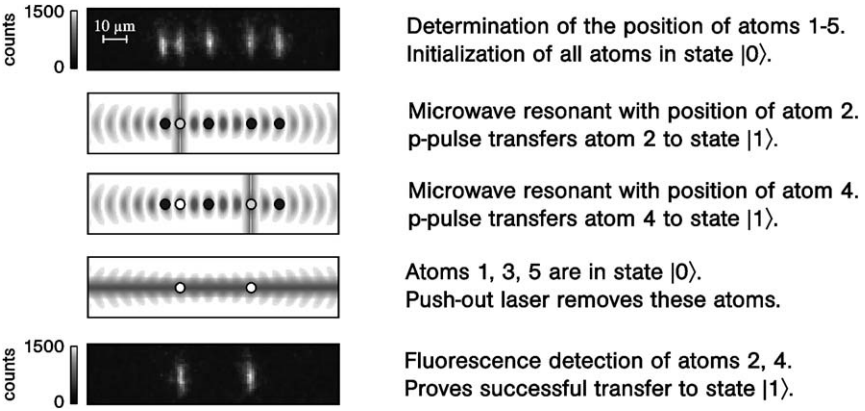

FIG. 11. Sequence of operations to generate and detect a $|01010\rangle$ quantum register state in a string of five atoms. The whole sequence lasts 1.5 s.

be used to create coherent superpositions of hyperfine states of the atoms trapped in our experiment [46]. However, in the experiments presented here, we use an alternative technique where we apply microwave radiation which is made resonant with an atom at a selected site only by means of magnetic field gradients. In this method, spatial selectivity is indeed realized in the same way as in magnetic resonance imaging (MRI) [50].

We can currently operate our register in the following way [51], see Fig. 11: We load between 2 and 10 atoms into our dipole trap. We then take a camera picture and determine the positions of all atoms with sub-micrometer precision. In the next step all atoms are optically pumped into the same $|F = 4, m_F = -4\rangle$ quantum state as described in Section 4 to initialize the register.

Individual addressing is now realized by tuning the microwave frequency to the exact transition frequency corresponding to the known individual atomic sites where the relationship is controlled by an external B-field gradient of $B' \simeq 0.15$ μT/μm along the DT axis. The atomic resonance frequency is shifted by the linear Zeeman effect according to $\nu = \nu_{\mathrm{hfs}} + 24.5$ kHz/μT, and we find a spatial frequency shift of $d\nu/dz = 3.7$ kHz/μm. We also apply a homogeneous magnetic field of about 0.4 mT in order to provide guiding for the angular momenta and to reduce the influence of transversal magnetic field gradients. In Fig. 11 we show the result of two selective inversion operations (π-pulses) carried out with a string of five atoms stored in our dipole trap array.

We have furthermore measured the resolution of the magnetic field gradient method. Figure 12 shows the result for the longest pulses applied (83 μs FWHM). The solid line is obtained from a numerical solution of the Bloch equations and reproduces the measurement very well. The spatial resolution is limited by the

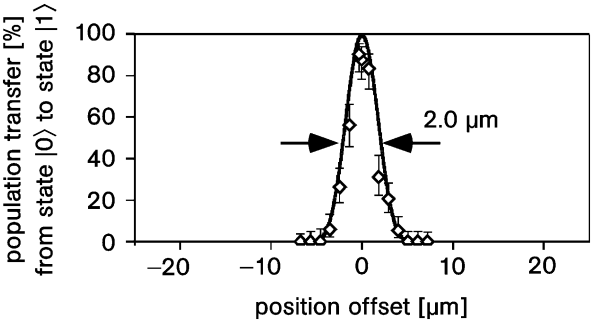

FIG. 12. Measured spatial resolution of the addressing scheme. The data were obtained by deliberately addressing positions offset from the actual atom site. For each point approximately 40 single atom events were analyzed. The Gaussian microwave π-pulse has a FWHM length of 83 μs.

Fourier width of the microwave pulse. Our method clearly demonstrates that we can address atoms for separations exceeding 2.5 μm (i.e., atoms are separated by about 5 empty sites). The resolution of the magnetic method in our current set-up is thus comparable to addressing by optical focusing. Neighboring atoms experience of course a phase shift due to non-resonant interaction with the microwave radiation. However, this phase shift is known and can be taken into account in further operations.

We have furthermore explored the coherence properties of atoms, now in the magnetically most sensitive $m_F = -4$ states instead of the $m_F = 0$ states. The results are displayed in Table I of Section 5. It is not surprising that dephasing times are much shorter in this case and are indeed dominated by fluctuations and inhomogeneities of the magnetic field. However, they are already now much larger than simple operation times for, e.g., π-pulses and technical improvements will further enhance the time available for coherent evolution.

The method described requires very precise timing of the microwave pulses in order to guarantee a precise control of the evolution from one quantum state to another. As an alternative, we have also applied quantum state control by means of rapid adiabatic passage [52]: In this case, the frequency of an intense microwave pulse is swept through resonance thereby transforming an initial into a final eigenstate of the system, in our case realized for the $|F = 4\rangle$ and $|F' = 3\rangle$ hyperfine ground states. In a gradient magnetic field we have analyzed the transfer probability as a function of the resonance position of the sweep center frequency with respect to the trapped atom for a fixed sweep width. The result in Fig. 13 shows the expected flat top profile indicating the reduced sensitivity to the precise setting of the center frequency and the sweep width [53]. The width of the edges which drop to zero within 3 μm is a measure of the spatial resolution of this method and comparable to the resonant addressing scheme described above.

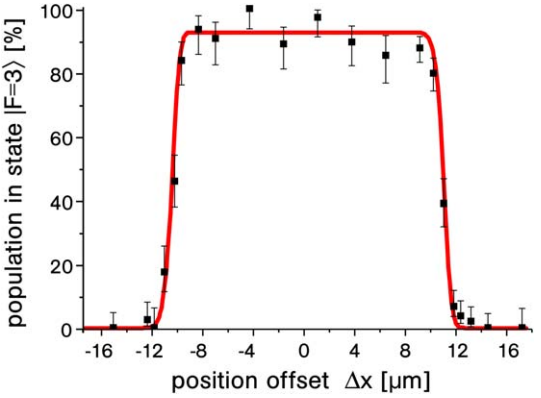

FIG. 13. Position-dependent adiabatic population transfer of individual atoms in an inhomogeneous magnetic field. The graph shows the population transfer as a function of the position offset Δx along the trap axis. Each data point is obtained from about 40 single atom measurements. The solid line is a theoretical fit [53].

Summarizing, in this section we have demonstrated procedures to experimentally realize both write and read operations at the level of a single neutral atom. We have demonstrated individual addressing of the atoms within a string of stored atoms with excellent resolution, and we are able to prepare arbitrary quantum superpositions on an individual atomic, or qubit site. In conclusion we have demonstrated the operation of a neutral atom quantum register, including the application of spin rotations, i.e., Hadamard gates in the language of quantum information processing.

8. Controlling the Atoms' Absolute and Relative Positions

Considering the ratio between the experimentally measured 2.5 μm addressing resolution presented above and the 1 mm Rayleigh zone of our standing wave DT, our neutral atom quantum register could in principle operate on more than 100 individually addressable qubits. Methods for the regularization of the distribution of atoms by controlling their absolute positions in the trap must be realized, however, in order to manage larger quantum registers. Tight position control is furthermore essential to realize the necessary controlled atom–atom interaction. In optical cavity QED, for example, this interaction is mediated by the field of an ultrahigh finesse Fabry–Perot resonator [36,54]. The field mode sustained by such a resonator has a typical transverse dimension of 10 μm so that the atom pair will have to be placed into this mode with a submicrometer precision while the

distance between the atoms has to be controlled at the same level. We have demonstrated such a submicrometer position control for individual neutral atoms [55].

8.1. An Optical Conveyor Belt

The position of the trapped atoms along the DT axis can be conveniently manipulated by introducing a relative detuning between the two counter-propagating dipole trap laser beams. A detuning by $\Delta\nu$ causes the standing wave pattern to move in the laboratory frame with a speed $\Delta\nu\lambda_{DT}/2$, where λ_{DT} is the wavelength of the DT laser. As a result, the trapping potential moves along the DT axis and thereby transports the atoms [56–58]. In the experiment, the relative detuning between the DT beams can be easily set with radiofrequency precision by acousto-optic modulators (AOMs, Fig. 4). They are placed in each beam and are driven by a phase-synchronous digital dual-frequency synthesizer. A phase slip of one cycle between the two trapping laser beams corresponds to a transportation distance of $\lambda_{DT}/2$.

We can realize typical accelerations of $a = 10{,}000\ \mathrm{m/s^2}$ and hence accelerate the atoms to velocities of up to 5 m/s (limited by the 10 MHz bandwidth of the AOMs) in half a millisecond. Thus, for typical parameters, a 1 mm transport takes about 1 ms. At the same time, the displacement of the atoms is controlled with a precision better than the dipole trap laser wavelength since this scheme allows us to control the relative phase of the two trapping laser beams to a fraction of a radian.

Using continuous illumination, we have imaged the controlled motion of one and the same or several atoms (Fig. 14) transported by the conveyor belt [58] with observation times exceeding one minute. Recently, it was shown that optical dipole traps similarly to our arrangement can be used to transport neutral atoms into high finesse resonators for cavity-QED experiments with very good precision [59,60].

8.2. Measuring and Controlling the Atoms' Positions

If one wants to take ultimate advantage of the optical conveyor belt transport above in order to place atoms at a predetermined position, the atoms' initial position along the dipole trap axis has to be known with the highest possible precision, ideally better than the distance between two adjacent potential wells. This can be achieved by recording and analyzing an ICCD fluorescence image of the trapped atoms. We have shown that by fitting the corresponding fluorescence peaks with a Gaussian, the atoms' position can be determined with a ± 150 nm precision from an ICCD image with 1 s exposure time [55].

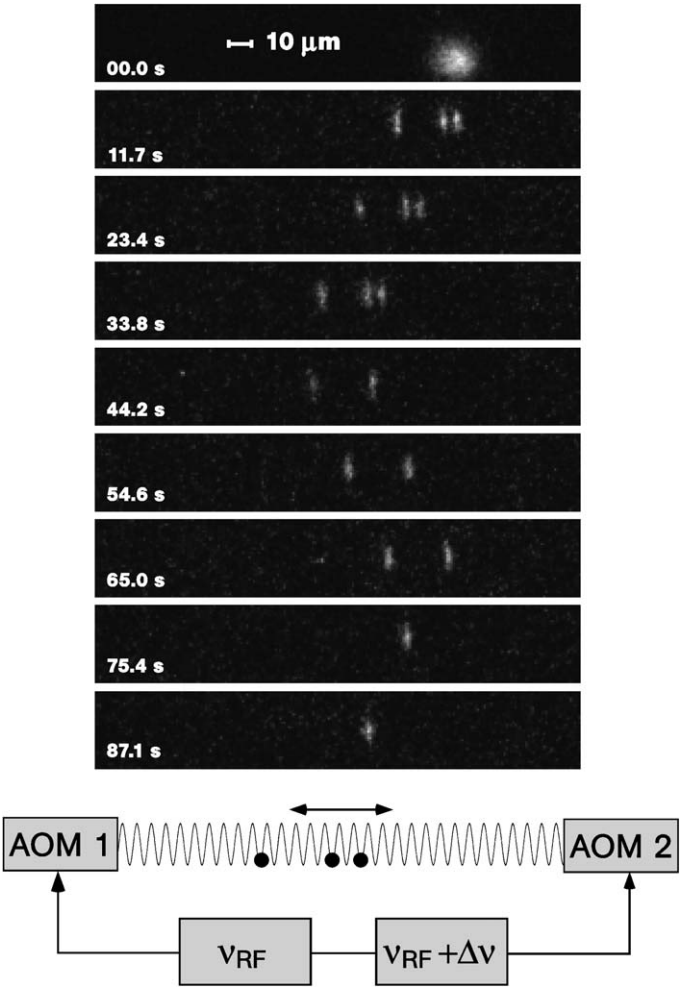

FIG. 14. Transport of 3 atoms by an optical conveyor belt: Snapshots of the movie published in [58]. In the first image, 3 atoms are stored in the MOT from where they are loaded into the conveyor belt formed by two counterpropagating laser beams. The frequency difference of the laser beams is controlled with two AOMs driven by a phase-coherent RF-source. At 40 s and 65 s the direction of transport is reversed. The atoms are lost from the conveyor belt by random collisions with thermal residual gas.

Furthermore, we have demonstrated that by means of our optical conveyor belt technique, we can place an atom at a predetermined position along the dipole trap axis with a ± 300 nm accuracy. Such a position control sequence is exemplified in

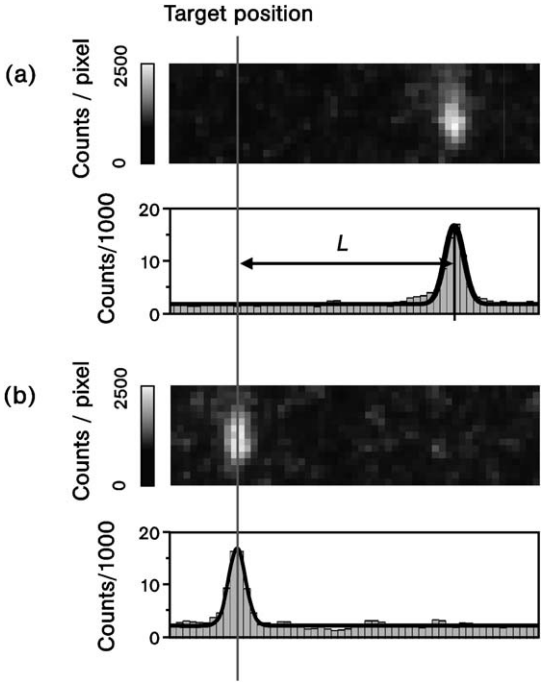

FIG. 15. Active position control. (a) After transferring a single atom from the MOT into the dipole trap its initial position is determined from an ICCD image and its distance with respect to the target position is calculated. (b) The atom is then transported to the target position and its final position is again measured from an ICCD image.

Fig. 15. After loading one atom from the MOT into the dipole trap, its position has a ± 5 μm uncertainty, corresponding to the diameter of the MOT. We determine the atom's initial position from a first ICCD fluorescence image and calculate its distance L from the desired target position. The atom is then transported to this target position and the success of the operation is verified by means of a second ICCD image.

In order to measure the distance between two simultaneously trapped atoms, we determine their individual positions as above. From one such measurement with 1 s integration time, their distance can thus be inferred with a precision of $\sqrt{2} \times 150$ nm. This precision can even be further increased by taking more than one image of the atom pair and by averaging over the measurements obtained from these images. Now, since the atoms are trapped inside a periodic potential, their distance d should be an integer multiple of the standing wave period: $d = n\lambda_{\mathrm{DT}}/2$; see Fig. 9(a). This periodicity is clearly visible in Fig. 16, where the cumulative distribution of atomic separations is given when averaging over more

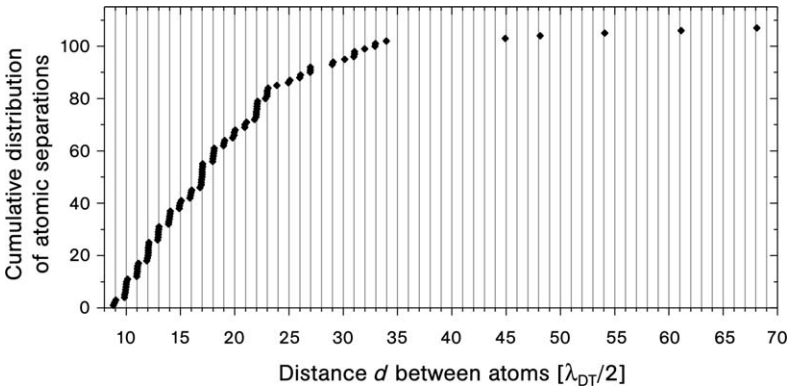

FIG. 16. Cumulative distribution of separations between simultaneously trapped atoms inside the standing wave potential. The discreteness of the atomic separations due to the standing wave potential is clearly visible.

than 10 distance measurements for each atom pair. The resolution of this distance measurement scheme is ±36 nm, much smaller than the standing wave period. We directly infer this value from the width of the vertical steps in Fig. 16. This result shows that we can determine the exact number of potential wells separating the simultaneously trapped atoms [55].

8.3. TWO-DIMENSIONAL POSITION MANIPULATION

A single standing wave optical dipole trap allows to shift the position of a string of trapped atoms as a whole in one dimension along the dipole trap axis using the optical conveyor belt technique presented above. If one seeks to prepare strings with a well-defined spacing or to rearrange the order of a string of trapped atoms, however, a two-dimensional manipulation of the atomic positions is required. For this reason, we have set up a second standing wave dipole trap, perpendicular to the first one, which acts as optical tweezers and which allows us to extract atoms out of a string and to reinsert them at another predefined position.

Figure 17 shows a first preliminary result towards this atom sorting and distance control scheme [61]. We start with a string of three randomly spaced atoms which has been loaded from the MOT into the horizontal (conveyor belt) dipole trap. In Fig. 17(a), the string has already been shifted such that the rightmost atom is placed at the position of the vertical (optical tweezers) dipole trap. This atom is then extracted with the vertical dipole trap and, after shifting the remaining two atoms along the horizontal dipole trap, we place it 15 μm to the left of the initially leftmost atom of the string; see Figs. 17(b)–(d). Repeating this procedure a second time, we prepare a string of three equidistantly spaced atoms, where the order of

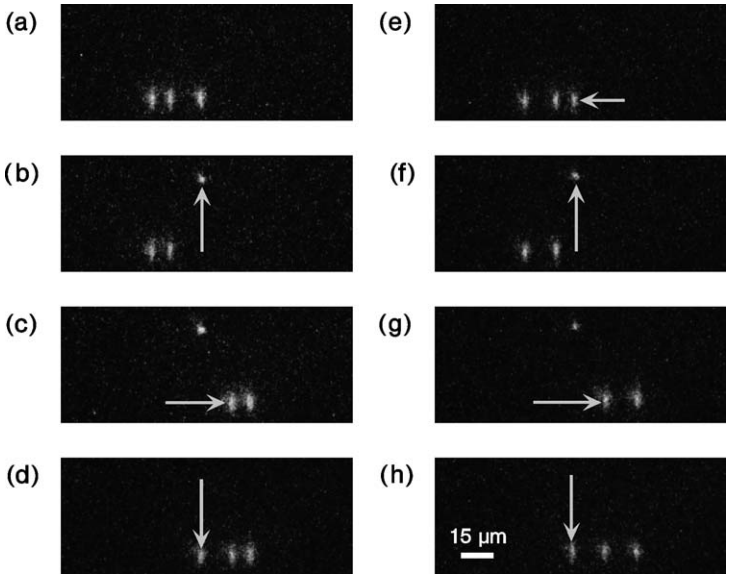

FIG. 17. Rearranging a string of three atoms using two perpendicular standing wave dipole traps. See text for details.

the string has been modified according to $(1, 2, 3) \rightarrow (3, 1, 2) \rightarrow (2, 3, 1)$; see Figs. 17(e)–(h).

9. Towards Entanglement of Neutral Atoms

There is a plentitude of proposals of how to implement a two-qubit quantum gate with neutral atoms which suggest the coherent photon exchange of two atoms inside a high-finesse optical resonator [36,54,59,62]. The experimental challenges for their realization are quite demanding. Although there has been a number of successes in optical cavity-QED research recently, including the transport of atoms into a cavity [59,60], trapping of single atoms inside a cavity [63], single photon generation [64,65], feedback control of the atomic motion in a cavity [66,67], and cooling of atoms inside a cavity [68–70], the realization of a two-qubit quantum gate with ground state atoms remains to be shown.

9.1. AN OPTICAL HIGH-FINESSE RESONATOR FOR STORING PHOTONS

Our goal is the deterministic placement of two atoms inside an optical high-finesse resonator. For this purpose, we have already set up and stabilized a suitable res-

onator [71]. We plan to transport atoms from the MOT, which is a few millimeters away from the cavity, into the cavity mode using our optical conveyor belt. Employing the imaging techniques and the image analysis presented above, we were recently able to control the position of the trapped atoms along the trap axis with a precision of ±300 nm [55]. This should allow us to reliably place the atoms into the center of the cavity mode, which has a diameter of 10 μm. Since the microwave-induced one-qubit operations on the quantum register demonstrated in Section 7 do not require optical access to the trapped atoms, they can even take place inside the cavity.

9.2. A Four-Photon Entanglement Scheme

One of the most promising schemes to create entanglement between two atoms in optical cavity QED was proposed by L. You et al. [54] and is the basis for the realization of a quantum phase gate [72]. It relies on the coherent energy exchange between two atoms stimulated by a four-photon Raman process involving the cavity mode and an auxiliary laser field. We have determined optimized theoretical parameters and calculated the expected fidelity according to this proposal for our particular experimental conditions. With a maximum fidelity of $F = 85\%$, which can be expected from this calculation. The demonstration of entanglement and the implementation of a quantum gate thus seems feasible with our experimental apparatus.

9.3. Cold Collisions in Spin-Dependent Potentials

We plan to investigate small strings of collisionally interacting neutral atoms for applications in quantum information processing. The atoms are stored, one by one, in a standing wave dipole trap and the interaction between the atoms, necessary for the implementation of quantum gates, will be realized through controlled cold collisions [39,40] which have been demonstrated with large sample of ultracold atoms already but without addressability of the individual atomic qubit [15]. For this purpose, we will employ the technique of spin dependent transport [39,40] at the level of individual atoms. This technique will allows us to "manually" split the wave functions of the trapped atoms in a deterministic and fully controlled single atom Stern–Gerlach experiment, where the dipole trap provides the effective magnetic field. By recombining the atomic wave function, we will then realize a single atom interferometer and directly measure the coherence properties of the splitting process. A sequence of splitting operations, carried out on a single atom, will result in a quantum analogue of the Galton board, where the atom carries out a quantum walk. Such quantum walks have recently been proposed as an alternative approach to quantum computing [73]. Our ultimate goal

is the implementation of fundamental quantum gates using controlled cold collisions within a register of 2–10 trapped neutral atoms. A parallel application of such quantum gates should then open the route towards the preparation of small cluster states [74] consisting of up to 10 individually addressable qubits.

10. Conclusions

In this overview, we have presented experimental techniques and results concerning the preparation and manipulation of single or a few optically trapped neutral Caesium atoms. We have shown that a specially designed magneto-optical trap (MOT) can store a countable number of atoms. Information about the dynamics of these atoms inside the MOT can be gained at all relevant timescales by analyzing photon correlation in their resonance fluorescence. Furthermore, using active feedback schemes, the Poissonian fluctuations of the number of atoms in the MOT can be overcome, making such a MOT a highly deterministic source of an exactly known number of cold atoms.

For coherent manipulation, we transfer the atoms with a high efficiency from the dissipative MOT into the conservative potential of a standing wave dipole trap (DT). The quantum state of atoms stored in this DT can be reliably prepared and detected at the level of single atoms. We have examined the coherence properties of the atoms in the DT and identified the dephasing mechanisms in this system. The experimentally measured long coherence times show that the atomic hyperfine ground states are well suited for encoding and processing coherent information.

A string of such trapped Caesium atoms has thus been used to realize a quantum register, where individual atoms were addressed with microwave pulses in combination with a magnetic field gradient. Using this method, we have demonstrated all basic register operations: initialization, selective addressing, coherent manipulation, and state-selective detection of the individual atomic states.

We have furthermore demonstrated a high level of control of the atoms' external degrees of freedom. Our DT can be operated as an "optical conveyor belt" that allows to move the atoms with submicrometer precision along the DT. In addition, we have measured the absolute and relative positions of the atoms along the dipole trap with a submicrometer accuracy. This high resolution allows us to measure the exact number of potential wells separating simultaneously trapped atoms in our 532 nm-period standing wave potential and to transport an atom to a predetermined position with a suboptical wavelength precision.

Finally, using a second dipole trap operated as optical tweezers, we have obtained first results towards an active control of the atoms' relative positions within the string. This will allow us to prepare strings with a preset interatomic spacing and to rearrange the order of atoms within the string at will.

The presented techniques are compatible with the requirements of cavity QED and controlled cold collision experiments. In our laboratory, we now actively work towards the implementation of such experiments in order to realize quantum logic operations with neutral ground state atoms.

11. Acknowledgements

We wish to thank the Deutsche Forschungsgemeinschaft, the Studienstiftung des Deutschen Volkes, the Deutsche Telekom Stiftung, INTAS, and the European Commission for continued support. Furthermore, we are indebted to numerous enthusiastic coworkers and students at the Diplom- and doctoral level who have participated in this research: W. Alt, K. Dästner, I. Dotsenko, L. Förster, D. Frese, V. Gomer, D. Haubrich, M. Khudaverdyan, S. Knappe, S. Kuhr, Y. Miroshnychenko, S. Reick, U. Reiter, W. Rosenfeld, H. Schadwinkel, D. Schrader, F. Strauch, B. Ueberholz, and R. Wynands.

12. References

[1] W. Neuhauser, M. Hohenstatt, P. Toschek, H. Dehmelt, *Phys. Rev. A* **22** (1980) 1137.
[2] W. Nagourney, J. Sandberg, H. Dehmelt, *Phys. Rev. Lett.* **56** (1986) 2797.
[3] J. Bergquist, R. Hulet, W. Itano, D. Wineland, *Phys. Rev. Lett.* **56** (1986) 1699.
[4] T. Sauter, W. Neuhauser, R. Blatt, P. Toschek, *Phys. Rev. Lett.* **56** (1986) 1696.
[5] F. Diedrich, H. Walther, *Phys. Rev. Lett.* **58** (1987) 203.
[6] F. Diedrich, E. Peik, J.M. Chen, W. Quint, H. Walther, *Phys. Rev. Lett.* **59** (1987) 2931.
[7] D. Wineland, J. Bergquist, W. Itano, J. Bollinger, C. Manney, *Phys. Rev. Lett.* **59** (1987) 2935.
[8] Z. Hu, H.J. Kimble, *Opt. Lett.* **19** (1994) 1888.
[9] D. Haubrich, H. Schadwinkel, F. Strauch, B. Ueberholz, R. Wynands, D. Meschede, *Europhys. Lett.* **34** (1996) 663.
[10] F. Ruschewitz, D. Bettermann, J.L. Peng, W. Ertmer, *Europhys. Lett.* **34** (1996) 651.
[11] For an overview see: H. Metcalf, P. van der Straaten, "Laser Cooling and Trapping", Springer, Heidelberg, 1999.
[12] M. Anderson, J. Ensher, M. Matthews, C. Wieman, E. Cornell, *Science* **269** (1995) 198.
[13] C. Pethick, H. Smith, "Bose–Einstein Condensation in Dilute Gases", Cambridge University Press, Cambridge , 2002.
[14] M. Greiner, O. Mandel, T. Esslinger, T.W. Hansch, I. Bloch, *Nature* **415** (2002) 39.
[15] O. Mandel, M. Greiner, A. Widera, T. Rom, T. Hänsch, I. Bloch, *Nature* **425** (2003) 937.
[16] For an overview see: R. Miller, T. Northup, K. Birnbaum, A. Boca, A. Boozer, H.J. Kimble, *J. Phys. B: At. Mol. Opt. Phys.* **38** (2005) 551–565.
[17] E. Rab, M. Prentiss, A. Cable, S. Chu, D. Pritchard, *Phys. Rev. Lett.* **59** (1987) 2631.
[18] C. Monroe, W. Swann, H. Robinson, C. Wieman, *Phys. Rev. Lett.* **65** (1990) 1571.
[19] D. Haubrich, A. Höpe, D. Meschede, *Opt. Comm.* **102** (1993) 225.
[20] W. Alt, *Optik* **113** (2002) 142.
[21] Z.-T. Lu, K.D.A. Wendt, *Rev. Sci. Instr.* **74** (2003) 1169.
[22] R. Hanbury Brown, R.Q. Twiss, *Nature* **177** (1956) 27.

[23] V. Gomer, D. Meschede, *Ann. Phys. (Leipzig)* **10** (2001) 9, and references therein.
[24] H.J. Kimble, M. Dagenais, L. Mandel, *Phys. Rev. Lett.* **39** (1977) 691.
[25] J. Dalibard, C. Cohen-Tannoudji, *J. Opt. Soc. Am. B* **6** (1989) 2023.
[26] D. Weiss, E. Riis, Y. Shevy, P. Jeffrey Ungar, S. Chu, *J. Opt. Soc. Am. B* **6** (1989) 2058.
[27] B. Ueberholz, S. Kuhr, D. Frese, V. Gomer, D. Meschede, *J. Phys. B: At. Mol. Opt. Phys.* **35** (2002) 4899.
[28] P.S. Julienne, A.M. Smith, K. Burnett, *Adv. At. Mol. Opt. Phys.* **30** (1993) 141.
[29] N. Schlosser, G. Reymond, I. Protsenko, P. Grangier, *Nature* **411** (2001) 1024.
[30] P. Willems, R. Boyd, J. Bliss, K. Libbrecht, *Phys. Rev. Lett.* **78** (1997) 1660.
[31] S.B. Hill, J.J. McClelland, *Appl. Phys. Lett.* **82** (2003) 3128.
[32] Y. Miroshnychenko, W. Alt, I. Dotsenko, L. Förster, M. Khudaverdyan, D. Meschede, S. Reick, D. Schrader, A. Rauschenbeutel, in preparation.
[33] D. Frese, B. Ueberholz, S. Kuhr, W. Alt, D. Schrader, V. Gomer, D. Meschede, *Phys. Rev. Lett.* **85** (2000) 3777.
[34] W. Alt, D. Schrader, S. Kuhr, M. Müller, V. Gomer, D. Meschede, *Phys. Rev. A* **67** (2003) 033403.
[35] D.P. DiVicenzo, *Fortschr. Phys.* **48** (2000) 771.
[36] T. Pellizari, S. Gardiner, J. Cirac, P. Zoller, *Phys. Rev. Lett.* **75** (1995) 3788.
[37] S.B. Zheng, G.C. Guo, *Phys. Rev. Lett.* **85** (2000) 2392.
[38] S. Osnaghi, P. Bertet, A. Auffeves, P. Maioli, M. Brune, J.M. Raimond, S. Haroche, *Phys. Rev. Lett.* **97** (2001) 037902.
[39] G. Brennen, C.M. Caves, P.S. Jessen, I.H. Deutsch, *Phys. Rev. Lett.* **82** (1999) 1060.
[40] D. Jaksch, H.-J. Briegel, J.I. Cirac, C.W. Gardiner, P. Zoller, *Phys. Rev. Lett.* **82** (1999) 1975.
[41] S. Kuhr, W. Alt, D. Schrader, I. Dotsenko, Y. Miroshnychenko, A. Rauschenbeutel, D. Meschede, *Phys. Rev. A* **72** (2005) 023406.
[42] N. Davidson, H.J. Lee, C.S. Adams, M. Kasevich, S. Chu, *Phys. Rev. Lett.* **74** (1995) 1311.
[43] N. Ramsey, "Molecular Beams", Oxford University Press, London, 1956.
[44] S. Kuhr, W. Alt, D. Schrader, I. Dotsenko, Y. Miroshnychenko, W. Rosenfeld, M. Khudaverdyan, V. Gomer, A. Rauschenbeutel, D. Meschede, *Phys. Rev. Lett.* **91** (2003) 213002.
[45] M.F. Andersen, A. Kaplan, N. Davidson, *Phys. Rev. Lett.* **90** (2003) 023001.
[46] I. Dotsenko, W. Alt, S. Kuhr, D. Schrader, M. Müller, Y. Miroshnychenko, V. Gomer, A. Rauschenbeutel, D. Meschede, *Appl. Phys. B* **78** (2004) 711.
[47] H.C. Nägerl, D. Leibfried, H. Rohde, G. Thalhammer, J. Eschner, F. Schmidt-Kaler, R. Blatt, *Phys. Rev. A* **60** (1999) 145.
[48] F. Schmidt-Kaler, H. Häffner, M. Riebe, S. Gulde, G.P.T. Lancaster, T. Deuschle, C. Becher, C.F. Roos, J. Eschner, R. Blatt, *Nature* **422** (2003) 408.
[49] D. Leibfried, B. DeMarco, V. Meyer, D. Lucas, M. Barrett, J. Britton, W.M. Itano, B. Jelenkovic, C. Langer, T. Rosenband, D.J. Wineland, *Nature* **422** (2003) 412.
[50] P.C. Lauterbur, *Nature* **242** (1973) 190.
[51] D. Schrader, I. Dotsenko, M. Khudaverdyan, Y. Miroshnychenko, A. Rauschenbeutel, D. Meschede, *Phys. Rev. Lett.* **93** (2004) 150501.
[52] N.V. Vitanov, M. Fleischhauer, B.W. Shore, K. Bergmann, *Adv. At. Mol. Opt. Phys.* **46** (2001) 55.
[53] M. Khudaverdyan, W. Alt, I. Dotsenko, L. Förster, S. Kuhr, D. Meschede, Y. Miroshnychenko, D. Schrader, A. Rauschenbeutel, *Phys. Rev. A* **71** (2005) 031404(R).
[54] L. You, X.X. Yi, X.H. Su, *Phys. Rev. A* **67** (2003) 032308.
[55] I. Dotsenko, W. Alt, M. Khudaverdyan, S. Kuhr, D. Meschede, Y. Miroshnychenko, D. Schrader, A. Rauschenbeutel, *Phys. Rev. Lett.* **95** (2005) 033002.
[56] S. Kuhr, W. Alt, D. Schrader, M. Müller, V. Gomer, D. Meschede, *Science* **293** (2001) 278.
[57] D. Schrader, S. Kuhr, W. Alt, M. Müller, V. Gomer, D. Meschede, *Appl. Phys. B* **73** (2001) 819.
[58] Y. Miroshnychenko, D. Schrader, S. Kuhr, W. Alt, I. Dotsenko, M. Khudaverdyan, A. Rauschenbeutel, D. Meschede, *Opt. Express* **11** (2003) 3498.

[59] J.A. Sauer, K.M. Fortier, M.S. Chang, C.D. Hamley, M.S. Chapman, *Phys. Rev. A* **69** (2004) 097902.
[60] S. Nußmann, M. Hijlkema, B. Weber, F. Rohde, G. Rempe, A. Kuhn, *Phys. Rev. Lett.* **95** (2005) 173602.
[61] Y. Miroshnychenko, W. Alt, I. Dotsenko, L. Förster, M. Khudaverdyan, D. Meschede, D. Schrader, A. Rauschenbeutel, in preparation.
[62] C. Marr, A. Beige, G. Rempe, *Phys. Rev. A* **68** (2003) 033817.
[63] J. McKeever, A. Boca, A.D. Boozer, R. Miller, J.R. Buck, A. Kuzmich, H.J. Kimble, *Phys. Rev. Lett.* **90** (2003) 133602.
[64] A. Kuhn, M. Hennrich, G. Rempe, *Phys. Rev. Lett.* **89** (2002) 067901.
[65] J. McKeever, A. Boca, A.D. Boozer, R. Miller, J.R. Buck, A. Kuzmich, H.J. Kimble, *Science* **303** (2004) 1992.
[66] T. Fischer, P. Maunz, P.W.H. Pinkse, T. Puppe, G. Rempe, *Phys. Rev. Lett.* **88** (2002) 163002.
[67] D.A. Steck, K. Jacobs, H. Mabuchi, T. Bhattacharya, S. Habib, *Phys. Rev. Lett.* **92** (2004) 223004.
[68] H.W. Chan, A.T. Black, V. Vuletic, *Phys. Rev. Lett.* **90** (2003) 063003.
[69] P. Maunz, T. Puppe, I. Schuster, N. Syassen, P.W.H. Pinkse, G. Rempe, *Nature* **428** (2004) 50.
[70] S. Nußmann, K. Murr, M. Hijlkema, B. Weber, A. Kuhn, G. Rempe, *Nature Physics* (2005), in press.
[71] W. Alt, Ph.D. thesis, Universität Bonn, 2004.
[72] J. Preskill, *Proc. R. Soc. London, Ser. A* **454** (1998) 385.
[73] J. Kempe, *Contemp. Phys.* **44** (2003) 307.
[74] R. Raussendorf, H.J. Briegel, *Phys. Rev. Lett.* **86** (2001) 5188.